Available online at www.sciencedirect.com

jmr&t Journal of Materials Research and Technology

journal homepage: www.elsevier.com/locate/jmrt

Structural and superelastic properties of Fe–Mn–Al–Ni shape memory alloy sheets produced on industrial process routes by hot rolling

André Bauer [a,*], Malte Vollmer [a], Vincent Fabian Viebranz [b], Hans Jürgen Maier [b], Thomas Niendorf [a]

[a] Institute of Materials Engineering, University of Kassel, 34125 Kassel, Germany
[b] Institut für Werkstoffkunde (Materials Science), Leibniz Universität Hannover, 30823 Garbsen, Germany

ARTICLE INFO

Article history:
Received 20 February 2023
Accepted 28 April 2023
Available online 2 May 2023

Keywords:
Shape memory alloy
Mechanical properties
Abnormal grain growth
Martensitic phase transformation
FeMnAlNi
Industrial process route

ABSTRACT

In the present study the structural and functional properties of Fe–Mn–Al–Ni shape memory alloy sheets produced on an industrial process route focusing on hot rolling were investigated. The as-processed condition is characterized by a high fraction of the non-transforming γ-phase, which ensures good workability, but is associated with poor superelasticity. The alloy shows good structural properties with a yield strength of about 600 MPa, which is well above the usual transformation stress related to the martensitic phase transformation for the investigated alloy composition. After solution annealing, a microstructure showing no preferred orientation being characterized by distinctly larger grains is present. The results obtained reveal that the previous thermo-mechanical processing had no impact on the subsequent texture, however, provided a sufficient amount of driving force for abnormal grain growth. Imposed by a cyclic heat treatment, oligocrystalline structures with grain sizes above 10 mm can be achieved in the industrially processed material, which show superelastic properties similar to material processed in small batches in the laboratory.

1. Introduction

Shape memory alloys (SMAs) are a unique class of smart materials, which offer completely new design solutions for lightweight and sustainable constructions [1–5]. Through a reversible, stress-induced martensitic phase transformation, SMAs showing superelasticity are capable of accommodating very large strains several times while absorbing considerable energy [2]. These advantages make them very interesting for use as damping elements in many industrial sectors, such as civil engineering [3,4].

Currently, Ni–Ti-based SMAs are the most commonly used SMAs in industrial applications. However, the high costs of the alloying elements and the challenging machinability prevent their use for material-intensive applications [6,7]. Thus, Fe–Ni–Co-based SMAs, such as Fe–Ni–Co–Al–Ta–B [8], Fe–Ni–Co–Al–Ti [9], Fe–Ni–Co–Al–Ti–B [10,11],

* Corresponding author.
E-mail address: bauer@uni-kassel.de (A. Bauer).
https://doi.org/10.1016/j.jmrt.2023.04.260

Fe–Ni–Co–Al–Nb–B [12], and Fe–Mn-based SMAs, such as Fe–Mn–Si [13–15] and Fe–Mn–Al–Ni–X (X = Ti, Cr) [16–18], came into focus of research in recent years. In particular, the alloy system Fe–Mn–Al–Ni is characterized by promising superelastic properties [17–19]. Furthermore, Fe–Mn–Al–Ni exhibits a lower temperature dependence of the critical stress for martensitic transformation (0.53 MPa $°C^{-1}$ [18]) compared to Ni–Ti (5.7 MPa $°C^{-1}$ [18]). This significantly extends the range of service temperature and simplifies the use in new applications.

The superelastic properties of Fe–Mn–Al–Ni strongly depend on size, volume fraction and interparticle distance of nanometric β-precipitates [19–22], which can be tailored by quenching rate, aging temperature and aging time. Quenching into 80 °C warm water followed by aging at 200 °C for 3 h has proven to be suitable in several studies [23–26].

A major challenge of the alloy system is the strong dependence of the superelastic properties on grain orientation and grain size, which is a result of the pronounced anisotropy of transformation strains depending on grain orientation [18,27–30]. The anisotropy leads to severe incompatibilities at the grain boundaries in polycrystalline state, especially in the vicinity of triple junctions, leading to inferior superelastic behavior or even intergranular fracture [24,31]. Imposed by a cyclic heat treatment (CHT) between the α single-phase region and the α+γ two-phase region, abnormal grain growth (AGG) can be promoted and the grain size can be increased significantly resulting in an oligocrystalline structure or even single crystals of several centimeters in size [32]. In case of these microstructures no triple junctions are present, and the superelastic performance is enhanced significantly [32]. In single crystals as well as in oligocrystalline structures the predominating factor influencing the reversibility of the martensitic transformation is the orientation of the transforming grains [25,28,29,33]. On the one hand the orientation affects the transformation strain as well as the critical stress for the martensitic transformation, on the other hand it is strongly related to whether the martensite transforms in a twinned or detwinned type [25,33]. Orientations with large theoretical transformation strains, such as ⟨001⟩, tend to detwin under tension with increasing elongation, which is accompanied by the loss of reversibility [25,33]. In contrast, orientations near ⟨101⟩ retain the twinned martensite structure, and thus exhibit superior reversibility [25,33]. For single crystals with favorable orientations, superelastic strains up to 10% can be observed [19,32].

In many studies, the feasibility of industrial processing via conventional process routes used in steel industry is emphasized as an advantage of iron-based SMAs [5,16,34,35]. However, Fe–Mn–Al–Ni has never been processed on an

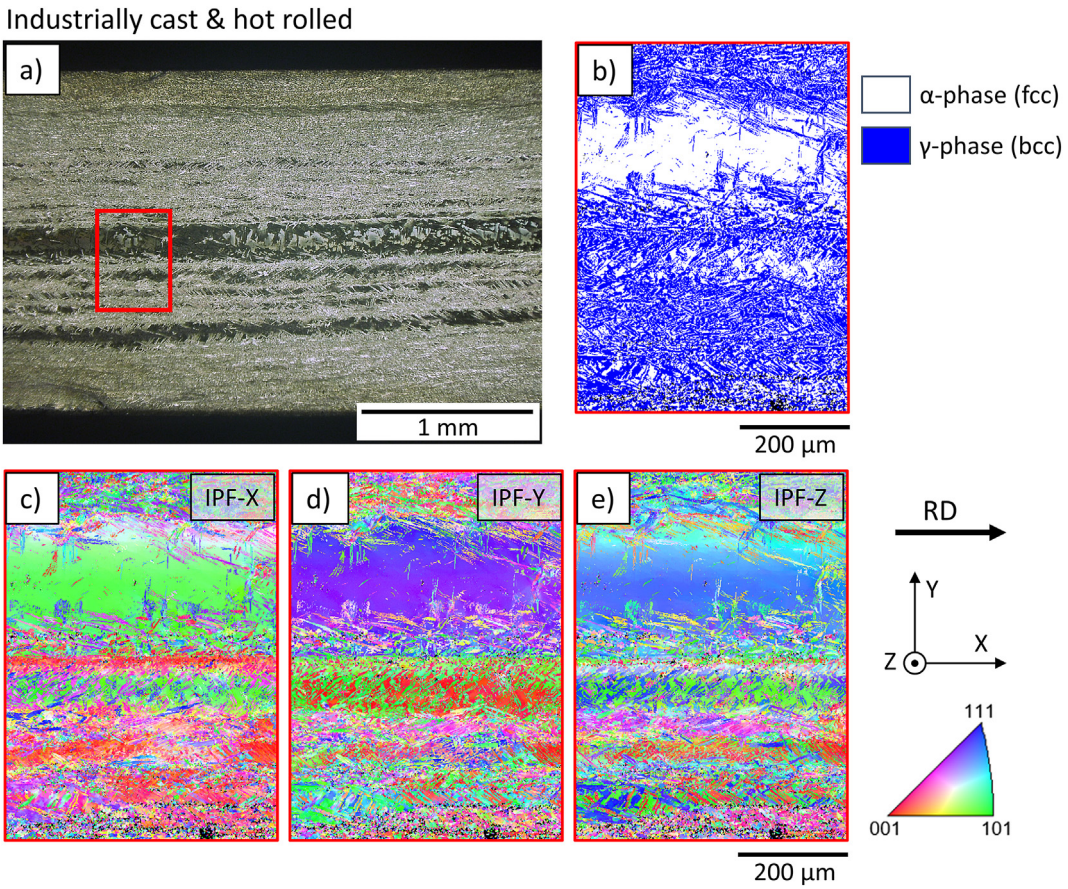

Fig. 1 – Microstructure of the industrial cast and hot rolled Fe–Mn–Al–Ni sheets: (a) micrograph showing the cross-section parallel to rolling direction (RD) in the hot rolled condition; (b) EBSD phase map of the area highlighted with a red box in (a); (c–e) EBSD orientation maps of the highlighted area for the corresponding directions X (RD), Y and Z.

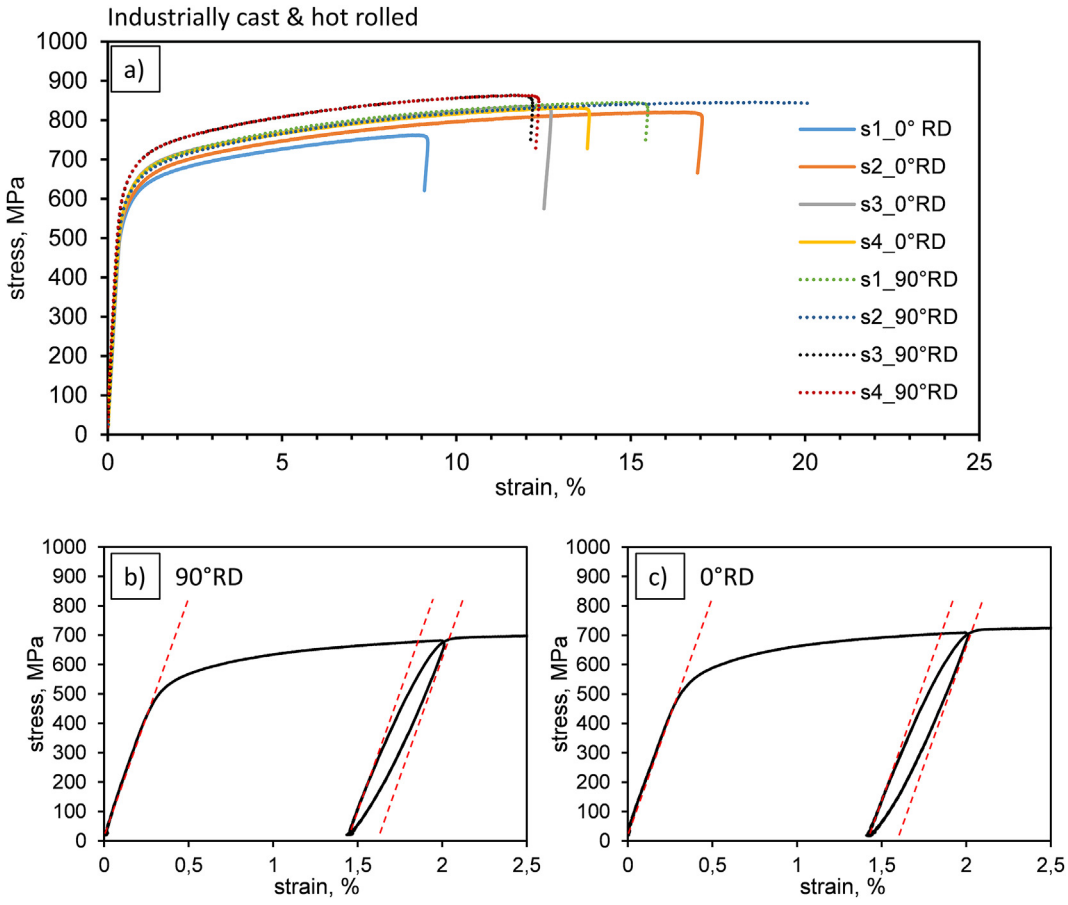

Fig. 2 – Mechanical properties in the hot rolled condition: (a) stress-strain curves obtained in tensile tests of 4 specimens, each extracted parallel to RD (0° RD) and perpendicular to RD (90° RD); (b) stress-stain curves obtained in incremental strain tests (IST) of specimens extracted perpendicular to RD (90° RD) and (c) parallel to RD (0° RD).

industrial production line so far. In the present study, Fe–Mn–Al–Ni was processed on an industrial test line for the first time, representing an industrial process route for the production of semi-finished sheets by hot rolling. The sheets were first characterized in the as-processed condition. Subsequently, it was evaluated whether the hot rolling procedure employed has an influence on microstructural evolution during post (cyclic) heat treatments. Microstructural characterization was carried out using electron backscatter diffraction (EBSD) and functional properties were investigated by *in situ* incremental strain tests (ISTs). The results are evaluated in direct comparison to literature values, the latter considering material produced using lab equipment.

2. Material and methods

The semi-finished sheet products investigated in this study were provided by thyssenkrupp Steel Europe AG (Duisburg, Germany), as part of a joint research project. For this purpose, Fe-32.9Mn-14.1Al-7.3Ni (at. %) sheets with a thickness of 2 mm were produced on an industrial test line by hot rolling. Details on processing parameters cannot be provided as these are intellectual property of the industry partner. The specified chemical composition of the sheet metal batch characterized in the present study was determined by Inductively Coupled Plasma-Optical Emission Spectrometry (ICP-OES).

To characterize the microstructure of the hot rolled condition, a square specimen of 15 mm × 3 mm from the center of the sheet was extracted by electro-discharge machining (EDM) with the long side parallel to the rolling direction (RD). The specimen was ground to a grit size of 5 μm and finally vibration-polished using a colloidal SiO_2 suspension with 0.02 μm particle size. Afterwards the specimen was etched using a solution of 3% nitric acid and 97% ethanol for optical microscopy.

For characterization of the mechanical behavior, dog-bone-shaped tensile specimens with a cross section of 2 mm × 1.6 mm and a gauge length of 18 mm were extracted by EDM. The specimens were ground to a grit size of 15 μm.

For subsequent heat treatments, the specimens were sealed into quartz tubes under argon atmosphere. A solution annealing was carried out at 1225 °C for 30 min with subsequent quenching into 80 °C warm water in order to study the effect of the thermo-mechanical process route on microstructural evolution. A cyclic heat treatment between the α single-phase region at 1225 °C and the α+γ two-phase region at 900 °C was carried out to obtain oligocrystalline

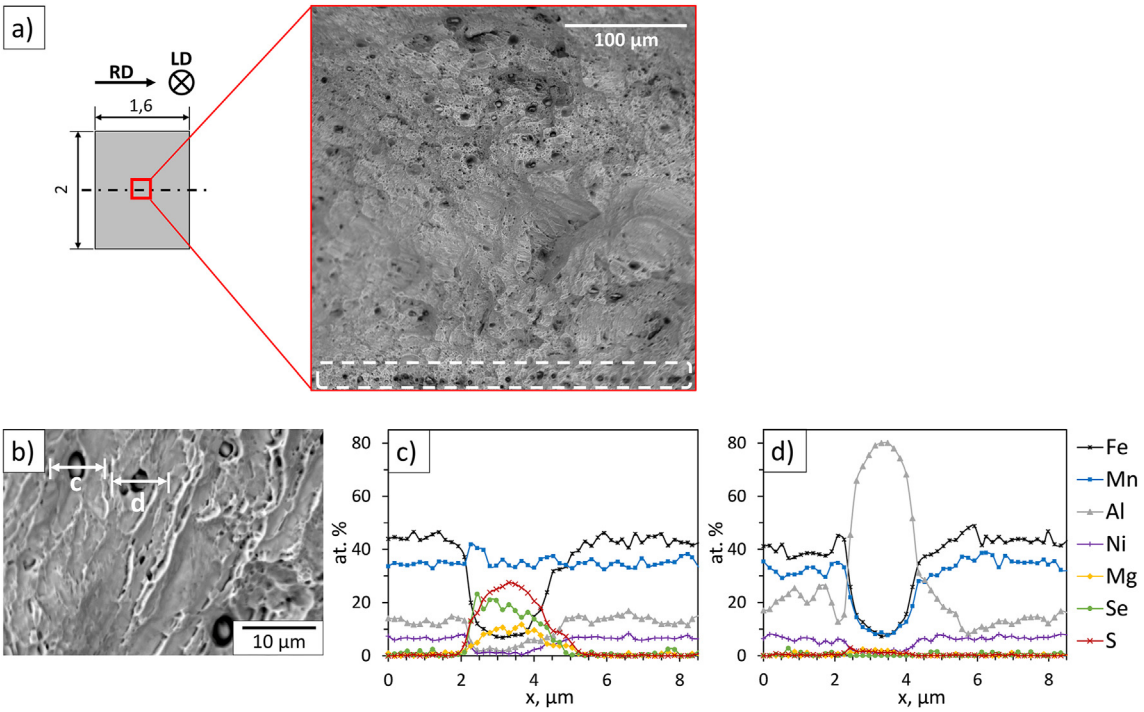

Fig. 3 – (a) SEM image of the characteristic distribution of inclusions at the fracture surfaces, where a cluster of inclusions is highlighted with a dashed box; (b) detailed view on some characteristic inclusions; (c–d) EDS line scans of the inclusions marked in (b).

structures by AGG. Three heat treatment cycles were conducted, each with a dwell time of 60 min at 1225 °C and 15 min at 900 °C. The heating and cooling ramps set were 5 K min^{-1}. After the final heat treatment cycle the specimens were quenched into 80 °C warm water and then directly aged at 200 °C for 3 h.

For the ISTs, the specimens were also ground to a grit size of 5 µm and vibration-polished. ISTs as well as tensile tests were carried out using a servo-hydraulic testing machine equipped with a 5 kN load cell. The tests were performed using a constant crosshead displacement of 5 µm s^{-1}. Strains were measured using an extensometer with a gauge length of 12 mm directly attached to the specimens. Images of the specimen surfaces in loaded and unloaded conditions were recorded using a digital optical microscope equipped with a tele-zoom objective.

Scanning electron microscopy (SEM) was used for in-depth microstructural characterization of the hot rolled, solution annealed and cyclic heat-treated condition. Electron backscatter diffraction (EBSD) analysis as well as energy dispersive X-ray spectroscopy (EDS) were performed with a nominal acceleration voltage of 20 kV.

3. Results and discussion

3.1. *Hot rolled condition*

Fig. 1a shows the cross-section of the Fe–Mn–Al–Ni sheet in the hot rolled condition. The micrograph already reveals an elongated microstructure parallel to RD. Fig. 1b shows the phase map of the area marked with a red box in Fig. 1a. In the middle of the cross-section an area, being predominantly characterized by the presence of the α-phase is visible. In the rest of the sheet cross-section a two-phase microstructure with a high fraction of γ-phase is present. The γ-phase forms in the selected temperature range of the hot rolling process and provides for a sufficient ductility, which is necessary for forming. In the EBSD orientation maps (Fig. 1c–e), different grain orientations are visible in the different layers of the sheet cross-section. Because of the high fraction of γ-phase, it is difficult to identify the shape of the α-grains. However, the grains seem to be slightly elongated in RD.

The mechanical tensile properties of the hot rolled condition are shown in Fig. 2a. The stress-strain curves indicate that no pronounced directional dependence is present. The average values for the 0.2% offset yield strength (σ_y) and tensile strength (UTS) in the specimens extracted perpendicular to RD (90° RD) are 625 MPa and 855 MPa, and thus slightly higher than the average values for the specimens extracted parallel to RD (0° RD), the latter being 585 MPa and 813 MPa, respectively. This is attributed to the stretched grains in rolling direction, resulting in a slightly smaller effective grain size perpendicular to rolling direction, eventually rationalizing the higher values for yield strength and tensile strength according to the Hall-Petch relation [36]. For the resulting strain at failure, pronounced scatter from 9% to 20% can be observed. This is assumed to be caused by non-metallic inclusions. Fracture surface analysis by SEM shows that many small spherical inclusions ranging from 1 µm to 5 µm in diameter are present at the fracture surfaces (Fig. 3a and b). EDS analysis reveals that there are two types of

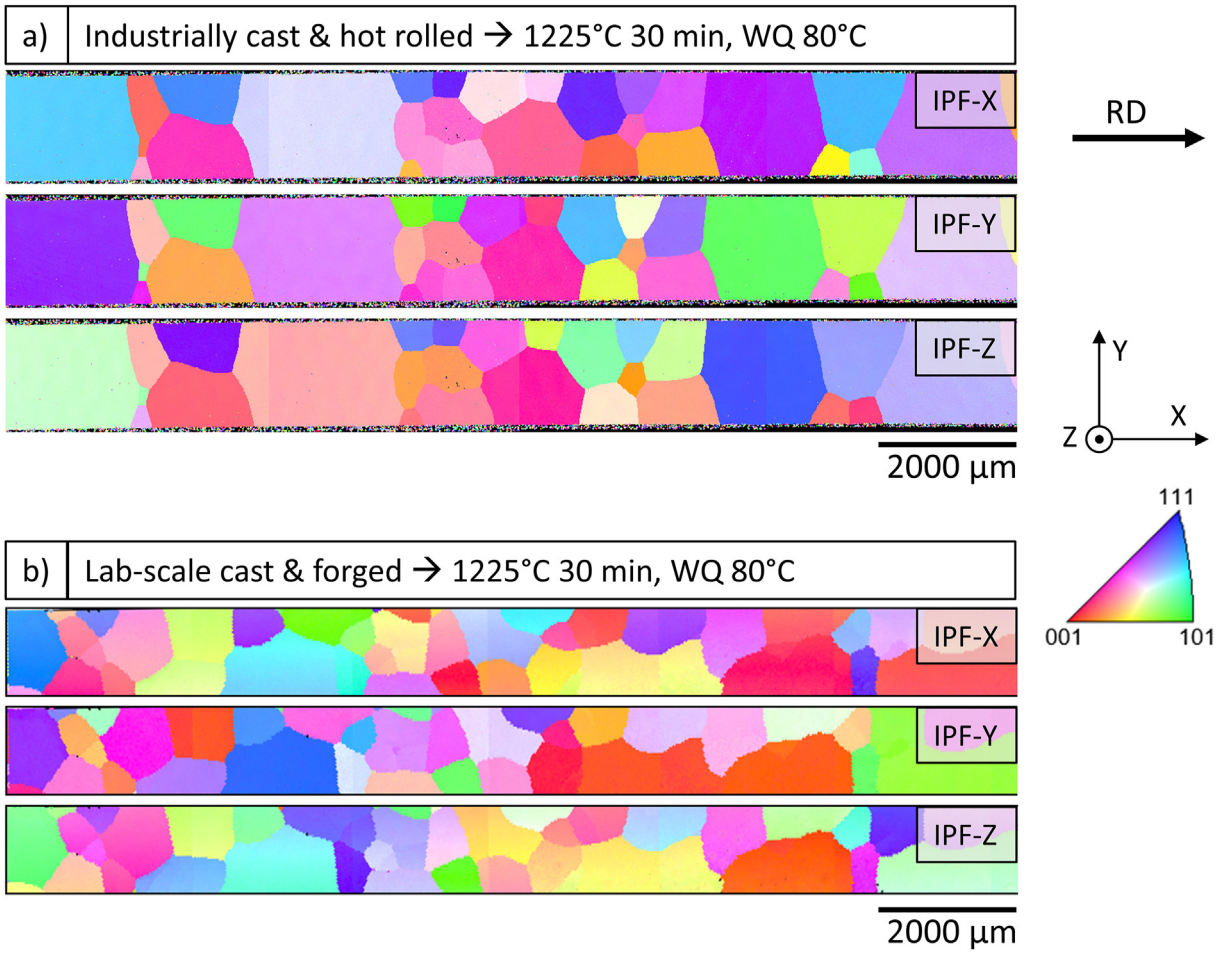

Fig. 4 – Influence of thermo-mechanical processing on microstructure after solution annealing: (a) EBSD orientation maps of a tensile specimen (extracted parallel to RD) of the industrial cast and hot rolled material batch after solution annealing at 1225 °C for 30 min followed by quenching into 80 °C warm water; (b) EBSD orientation maps of a tensile specimen of a lab-scale cast and forged material batch (recompiled from Ref. [40]).

inclusions. The first one has a high content of Mn, S and Se. Moreover, an increased amount of Mg can be detected within these inclusions (Fig. 3c). The second one consists mainly of Al (Fig. 3d). The latter appear to be AlN or Al_2O_3 inclusions. The occurrence of MnS(Se) as well as AlN and Al_2O_3 inclusions is well known from the production of twinning-induced plasticity steels, which also have a high content of Mn and Al [37]. Selenium is contained in electrolytic manganese, which is used as an alloying element in industrial production of high manganese steels [37]. Depending on volume fraction, size, distribution, composition and morphology of the inclusions, the mechanical properties can be strongly influenced [38]. Especially ductility is severely decreased with increasing amounts of oxides or sulfides, as these act as stress raisers [38]. The inclusions were observed in the fracture surfaces of all specimens and were present in a scattered fashion over the whole cross section. In the center of the cross section, some specimens showed a cluster of inclusions in a line parallel to rolling direction (Fig. 3a dashed box). However, no distinct differences in size, number and distribution of inclusions were observed between the specimens with low and high strain at failure. The most important results obtained from the ISTs are summarized in Fig. 2b and c. These indicate that there is almost no superelastic behavior in the hot rolled condition in both directions. This behavior had to be expected due to the high γ-phase content and the small grain size, both detrimentally affecting the fraction of transformable α-phase volume while introducing a vast number of obstacles for martensitic transformation. Therefore, a subsequent heat treatment with defined quenching conditions is required to obtain superelastic properties in case of the Fe–Mn–Al–Ni SMA.

3.2. *Solution annealed condition*

Due to the deformation introduced by hot rolling, recrystallization takes place during solution annealing, resulting in a polycrystalline microstructure showing no preferred orientation (Fig. 4a). It is obvious that the applied hot rolling process is not sufficient to induce a strong texture upon the subsequent heat treatment as the deformation degree upon hot rolling is too low. For Fe–Mn–Al–Ni, Ozcan et al. [39] showed that a

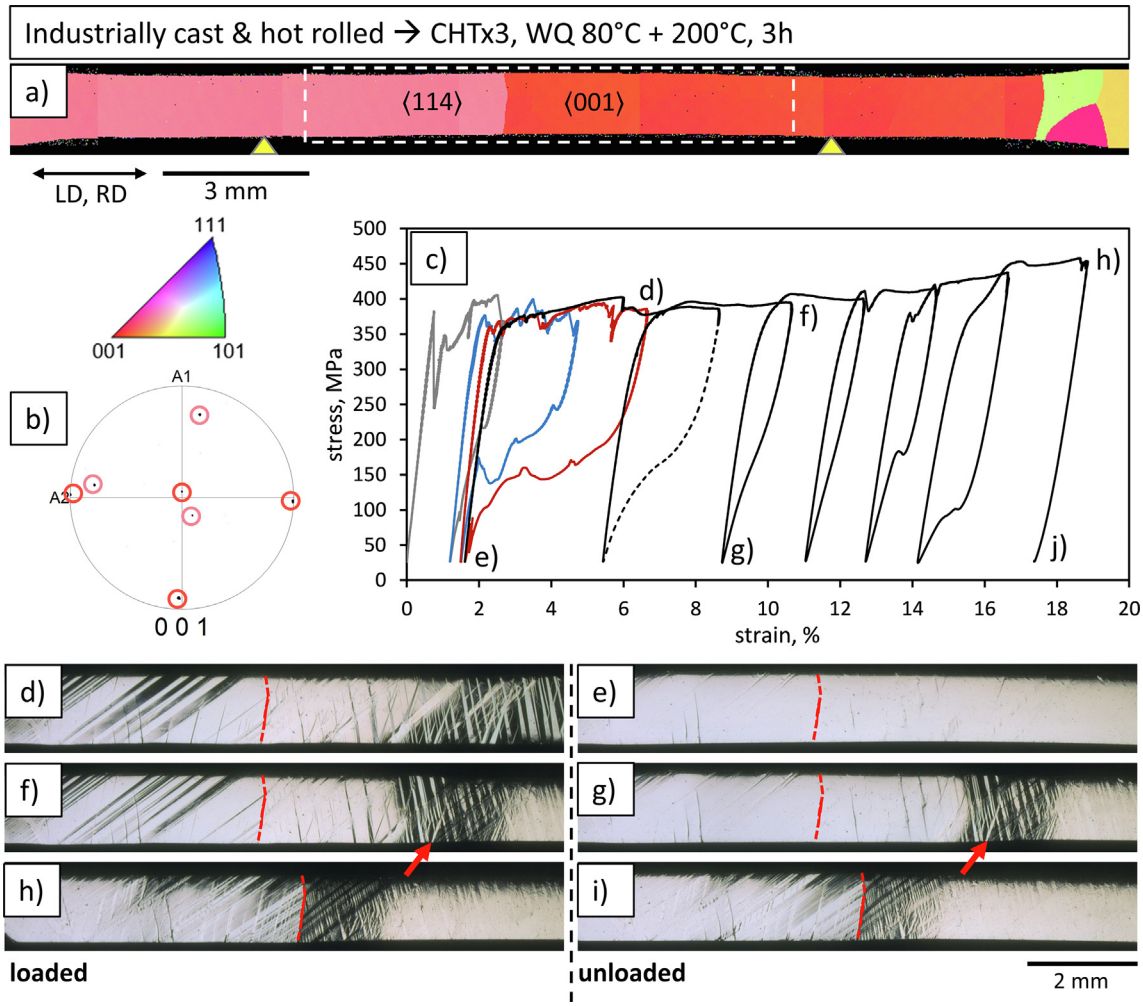

Fig. 5 – Superelastic behavior of the industrially cast and hot rolled Fe–Mn–Al–Ni sheet after cyclic heat treatment, subsequent quenching into 80 °C warm water and aging at 200 °C for 3 h: (a) EBSD orientation map of the tensile specimen plotted with respect to LD; the yellow triangles mark the positions at which the extensometer was placed; (b) corresponding pole figure for the grains involved in the martensitic transformation; (c) stress-strain curve of the depicted tensile specimen during the incremental strain test; (d–i) optical micrographs of the area highlighted with a white dotted box in (a) at different points of the load cycle; the red arrows in (f) and (g) mark the cross over from a necked area (right part) to a non-necked area (left part) of the specimen.

strong [110] recrystallization texture can be achieved upon cold wire drawing to an area reduction of 75%. Studies focusing on Fe–Ni–Co–Al–X (X = Ti [9], Ti–B [10,11], Nb–B [12]) SMAs revealed that a reduction ratio of more than 90% has to be achieved during cold rolling to obtain a distinct recrystallization texture. In the present study, the heterogeneous grain size distribution after solution annealing (Fig. 4a) has to be considered. Some grains already reached a size of about 2 mm, and thus span the entire specimen cross-section. A direct comparison to a lab-scale cast and forged material batch can be made taking into account the work of Vollmer et al. [40] (cf. Fig. 4b), where a more homogenous grain size distribution and smaller maximum grain sizes are visible after solution annealing at 1225 °C for 30 min (considering the same specimen geometry and identical procedure of heat treatment).

Therefore, hot rolling already seems to provide a sufficient driving force for AGG. It is known that subgrain structures resulting from dislocation rearrangements provide the main driving force for AGG during cyclic heat treatment [32]. The dislocations usually form as a result of growth of the semi-coherent γ-phase during cooling from the temperature of the α single-phase region into the α+γ two-phase region. The dislocations rearrange into subgrains during subsequent heating and remain in the α-parent-phase even after dissolution of the γ-phase [32]. Due to the additional energy induced by the subgrains, some grains grow much faster and consume the neighboring grains including subgrains [32].

By hot rolling in the temperature range of the two-phase region and subsequent solution annealing at 1225 °C, the material has undergone a temperature history similar to one cycle of the cyclic heat treatment according to Omori et al. [32]. In addition, it can be expected that dislocations were formed during the deformation process, influencing the resulting

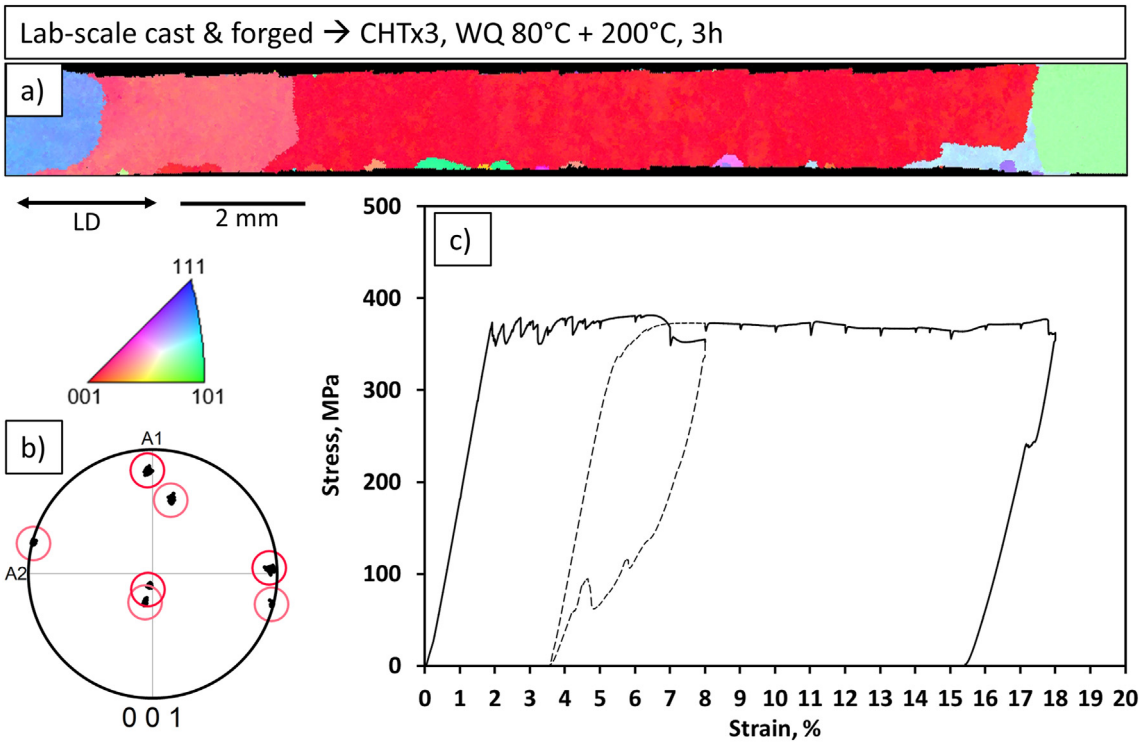

Fig. 6 – Superelastic behavior of a lab-scale cast and forged material batch after cyclic heat treatment, subsequent quenching into 80 °C warm water and aging at 200 °C for 3 h: (a) EBSD orientation map of the tensile specimen plotted with respect to LD; (b) corresponding pole figure for the grains involved in martensitic transformation; (c) stress-strain curve of the depicted tensile specimen up to 18% applied strain (recompiled from Ref. [25]).

subgrain structures. Vollmer et al. [16] revealed that the morphology of the γ-phase has a strong influence on the resulting subgrain size and, eventually, on the grain growth rate. A refinement of the formed γ-phase and subgrains can significantly promote AGG [16]. This can be achieved by changing the chemical composition, such as adding titanium [16] or increasing the aluminum content [41]. Due to hot rolling, the γ-phase also exhibits a much finer morphology, which likely also boosts AGG. It should be noted, however, that the additional driving force introduced by hot rolling, in contrast to tailoring the chemical composition, can only take effect on grain growth behavior during the first solution annealing step at the beginning of the cyclic heat treatment. After solution annealing at 1225 °C, the fine γ-phase precipitates as well as the dislocation structures induced by hot rolling should be completely dissolved. Thus, the previous process route, i.e. the hot rolling, has no remarkable further influence on the AGG in the subsequent steps of a cyclic heat treatment. In contrast, the adjustment of the chemical composition, e.g. by the addition of Ti [16], has a permanent effect on the morphology of the γ precipitates, and thus on the size of the resulting subgrains and the driving force for the AGG during each heat treatment cycle.

3.3. *Cyclic heat-treated condition*

After cyclic heat treatment a bamboo-like microstructure with grain sizes above 10 mm is visible (Fig. 5a). The microstructure and the grain orientations of the specimen are very similar compared to a specimen of a lab-scale processed Fe–Mn–Al–Ni material batch shown in Fig. 6a. Specifically, the grain orientations involved in martensitic transformation are nearly identical. The stress-strain curves obtained in the IST are shown in Fig. 5c. A first martensitic transformation takes place at a stress level of 382 MPa and is followed by an initial stress drop to 250 MPa, followed by further serrations in the stress-strain curve of the first loading cycle. Stress drops are linked to abrupt martensitic transformation of areas spanning the entire specimen cross-section. This transformation behavior has already been observed in several studies [24,26,39,42].

The reason for this specific transformation behavior, however, is not yet completely understood. Omori et al. [42] attributed the stress drops to nucleation barriers for martensitic plates and Ozcan et al. [39] observed that the size of the β-precipitates (B2) significantly influences the serrated flow behavior. With increasing size, the stress drops were also more pronounced. The influence of non-metallic inclusions present in the industrially processed material on martensitic transformation has not yet been considered. These inclusions might also act as barriers for martensitic transformation, which could explain the slightly more serrated stress-strain curve in the first loading cycles (Fig. 5c) compared to the lab-processed reference sample (cf. Fig. 6c). While the first transformation cycle is associated with a relatively high absolute value of irreversible deformation, the two subsequent cycles (blue and red curves in Fig. 5c) show an almost completely reversible transformation. The high reversibility of the third

cycle can also be deduced from the *in situ* images in the loaded (Fig. 5d) and unloaded state (Fig. 5e). A similar behavior was also observed in a previous study by Vollmer et al. [26] for a sample with the same grain orientation. Here, the first transformation seems to induce a high degree of dislocation activity. Thereby, the local stress states lead to a multi-variant martensitic transformation in the following load cycle, which at first glance seems to be supportive for good reversibility. However, the width of the stress-strain hysteresis is increased with each loading cycle, indicating cyclic degradation. In further load cycles of the IST reversibility decreased rapidly, starting at loading levels above 8% strain. The *in situ* images (Fig. 5f and g) show that the loss of reversibility is accompanied by macroscopic necking of the specimen (right side of the red arrow in Fig. 5f and g). This observation was also made in Ref. [25] and was linked to detwinning of the martensite. Even the specimen is completely functionally degraded at 18.7% strain, no structural failure occurs. With respect to the transformation stress (≈380 MPa) as well as reversibility of the transformation (≈2.8% superelastic strain after loading to about 8% total strain), the industrially processed material (Fig. 5) shows almost the same properties as the lab-scale processed material (Fig. 6) after cyclic heat treatment.

4. Conclusions

In the present study, the structural and functional properties of industrially processed Fe–Mn–Al–Ni sheets were investigated. The impact of the process route on microstructural evolution during post (cyclic) heat treatments as well as on the functional properties was studied in direct comparison to results of lab-scale processed material. Based on the results of the present study, the following conclusions can be drawn.

- Fe–Mn–Al–Ni semi-finished sheet products can be produced via industrial process routes well-established in steel industry using hot rolling.
- A high fraction of γ-phase is necessary to provide a sufficient ductility to achieve high deformation degrees during forming. However, this makes subsequent heat treatments necessary to obtain a functional behavior.
- The hot rolled condition is characterized by good structural properties featuring a yield strength of about 600 MPa, which is well above the transformation stress of the cyclic heat-treated condition (≈380 MPa). This opens up the opportunity to use the alloy as structural as well as functional material even in one component.
- The hot rolling process used does not induce a specific texture when post heat treatments are conducted. However, the formation of fine dispersed γ-precipitates and the deformation induced dislocations due to hot rolling seem to provide a driving force sufficient for abnormal grain growth.
- Imposed by a cyclic heat treatment, oligocrystalline structures with grain sizes above 10 mm can be established in the industrially processed material. Most importantly, the shape memory alloy studied shows almost identical superelastic properties as lab-scale processed material. This is shown for a near-⟨001⟩ grain orientation under tensile load with critical stresses for martensitic transformation of about 380 MPa and superelastic strains of 2.8% after loading to about 8% total strain.

Credit author statement

A. Bauer: Conceptualization, Methodology, Investigation, Visualization, Writing - original Draft.

M. Vollmer: Conceptualization, Methodology, Writing - review & editing.

V.F. Viebranz: Investigation, Writing - review & editing.

H.J. Maier: Conceptualization, Project administration, Funding acquisition, Review & editing.

T. Niendorf: Conceptualization, Project administration, Funding acquisition, Writing -review & editing.

Declaration of competing interest

The authors declare that they have no known competing financial interests or personal relationships that could have appeared to influence the work reported in this paper.

Acknowledgements

Financial support by Deutsche Forschungsgemeinschaft (project number 401738767) is gratefully acknowledged. The material was processed by thyssenkrupp Steel Europe AG (Duisburg, Germany).

REFERENCES

[1] Hartl DJ, Lagoudas DC. Aerospace applications of shape memory alloys. Proc Inst Mech Eng G J Aerosp Eng 2007;221(4):535–52. https://doi.org/10.1243/09544100JAERO211.

[2] Lagoudas DC. Shape memory alloys modeling and engineering applications. Boston, MA: Springer US; 2008.

[3] Song G, Ma N, Li H-N. Applications of shape memory alloys in civil structures. Eng Struct 2006;28(9):1266–74. https://doi.org/10.1016/j.engstruct.2005.12.010.

[4] Zareie S, Issa AS, Seethaler RJ, Zabihollah A. Recent advances in the applications of shape memory alloys in civil infrastructures: a review. Structures 2020;27(7):1535–50. https://doi.org/10.1016/j.istruc.2020.05.058.

[5] Zhang Z-X, Zhang J, Wu H, Ji Y, Kumar DD. Iron-based shape memory alloys in construction: research, applications and opportunities. Materials 2022;15(5). https://doi.org/10.3390/ma15051723.

[6] Kaya E, Kaya İ. A review on machining of NiTi shape memory alloys: the process and post process perspective. Int J Adv Des Manuf Technol 2019;100(5–8):2045–87.

[7] Mohd Jani J, Leary M, Subic A, Gibson MA. A review of shape memory alloy research, applications and opportunities. Mater Des 2014;56(1–2):1078–113. https://doi.org/10.1016/j.matdes.2013.11.084.

[8] Tanaka Y, Himuro Y, Kainuma R, Sutou Y, Omori T, Ishida K. Ferrous polycrystalline shape-memory alloy showing huge

superelasticity. Science 2010;327(5972):1488–90. https://doi.org/10.1126/science.1183169.
[9] Sobrero CE, Lauhoff C, Wegener T, Niendorf T, Krooß P. On the impact of texture and grain size on the pseudoelastic properties of polycrystalline Fe–Ni–Co–Al–Ti alloy. Shap Mem Superelasticity 2020;6(2):191–201. https://doi.org/10.1007/s40830-020-00280-4.
[10] Lee D, Omori T, Kainuma R. Ductility enhancement and superelasticity in Fe–Ni–Co–Al–Ti–B polycrystalline alloy. J Alloys Compd 2014;617:120–3. https://doi.org/10.1016/j.jallcom.2014.07.136.
[11] Lee D, Omori T, Han K, Hayakawa Y, Kainuma R. Effect of thermomechanical processing on texture and superelasticity in Fe–Ni-Co-Al–Ti-B alloy. Shap Mem Superelasticity 2018;4(1):102–11. https://doi.org/10.1007/s40830-018-0160-5.
[12] Fu H, Zhao H, Song S, Zhang Z, Xie J. Evolution of the cold-rolling and recrystallization textures in FeNiCoAlNbB shape memory alloy. J Alloys Compd 2016;686:1008–16. https://doi.org/10.1016/j.jallcom.2016.06.273.
[13] Dong Z, Klotz UE, Leinenbach C, Bergamini A, Czaderski C, Motavalli M. A novel Fe-Mn-Si shape memory alloy with improved shape recovery properties by VC precipitation. Adv Eng Mater 2009;11(1–2):40–4. https://doi.org/10.1002/adem.200800312.
[14] Hosseini E, Ghafoori E, Leinenbach C, Motavalli M, Holdsworth SR. Stress recovery and cyclic behaviour of an Fe–Mn–Si shape memory alloy after multiple thermal activation. Smart Mater Struct 2018;27(2):25009. https://doi.org/10.1088/1361-665X/aaa2c9.
[15] Sato A, Mori T. Development of a shape memory alloy Fe-Mn-Si. Mater Sci Eng, A 1991;146(1–2):197–204. https://doi.org/10.1016/0921-5093(91)90277-T.
[16] Vollmer M, Arold T, Kriegel MJ, Klemm V, Degener S, Freudenberger J, et al. Promoting abnormal grain growth in Fe-based shape memory alloys through compositional adjustments. Nat Commun 2019;10(1):2337. https://doi.org/10.1038/s41467-019-10308-8.
[17] Xia J, Noguchi Y, Xu X, Odaira T, Kimura Y, Nagasako M, et al. Iron-based superelastic alloys with near-constant critical stress temperature dependence. Science 2020;369(6505):855–8. https://doi.org/10.1126/science.abc1590.
[18] Omori T, Ando K, Okano M, Xu X, Tanaka Y, Ohnuma I, et al. Superelastic effect in polycrystalline ferrous alloys. Science 2011;333(6038):68–71. https://doi.org/10.1126/science.1202232.
[19] Vollmer M, Bauer A, Kriegel MJ, Motylenko M, Niendorf T. Functionally graded structures realized based on Fe–Mn–Al–Ni shape memory alloys. Scripta Mater 2021;194:113619. https://doi.org/10.1016/j.scriptamat.2020.10.057.
[20] Tseng LW, Ma J, Hornbuckle BC, Karaman I, Thompson GB, Luo ZP, et al. The effect of precipitates on the superelastic response of [1 0 0] oriented FeMnAlNi single crystals under compression. Acta Mater 2015;97:234–44. https://doi.org/10.1016/j.actamat.2015.06.061.
[21] Ozcan H, Ma J, Karaman I, Chumlyakov YI, Santamarta R, Brown J, et al. Microstructural design considerations in Fe-Mn-Al-Ni shape memory alloy wires: effects of natural aging. Scripta Mater 2018;142:153–7. https://doi.org/10.1016/j.scriptamat.2017.07.033.
[22] La Roca P, Baruj A, Sobrero CE, Malarría JA, Sade M. Nanoprecipitation effects on phase stability of Fe-Mn-Al-Ni alloys. J Alloys Compd 2017;708:422–7. https://doi.org/10.1016/j.jallcom.2017.02.280.
[23] Vollmer M, Kriegel MJ, Walnsch A, Klemm V, Leineweber A, Niendorf T. On the microstructural and functional stability of Fe-Mn-Al-Ni at ambient and elevated temperatures. Scripta Mater 2019;162:442–6. https://doi.org/10.1016/j.scriptamat.2018.12.008.
[24] Vollmer M, Segel C, Krooß P, Günther J, Tseng LW, Karaman I, et al. On the effect of gamma phase formation on the pseudoelastic performance of polycrystalline Fe–Mn–Al–Ni shape memory alloys. Scripta Mater 2015;108:23–6. https://doi.org/10.1016/j.scriptamat.2015.06.013.
[25] Bauer A, Vollmer M, Niendorf T. Effect of crystallographic orientation and grain boundaries on martensitic transformation and superelastic response of oligocrystalline Fe–Mn–Al–Ni shape memory alloys. Shape Memory and Superelasticity 2021;7(3):373–82. https://doi.org/10.1007/s40830-021-00340-3.
[26] Vollmer M, Krooß P, Kriegel MJ, Klemm V, Somsen C, Ozcan H, et al. Cyclic degradation in bamboo-like Fe–Mn–Al–Ni shape memory alloys — the role of grain orientation. Scripta Mater 2016;114:156–60. https://doi.org/10.1016/j.scriptamat.2015.12.007.
[27] Ojha A, Sehitoglu H. Transformation stress modeling in new Fe Mn Al Ni shape memory alloy. Int J Plast 2016;86(1):93–111. https://doi.org/10.1016/j.ijplas.2016.08.003.
[28] Tseng LW, Ma J, Chumlyakov YI, Karaman I. Orientation dependence of superelasticity in FeMnAlNi single crystals under compression. Scripta Mater 2019;166:48–52. https://doi.org/10.1016/j.scriptamat.2019.02.034.
[29] Tseng LW, Ma J, Wang SJ, Karaman I, Kaya M, Luo ZP, et al. Superelastic response of a single crystalline FeMnAlNi shape memory alloy under tension and compression. Acta Mater 2015;89(3):374–83. https://doi.org/10.1016/j.actamat.2015.01.009.
[30] Tseng LW. Microstructure and superelastic response of iron-based shape memory alloys. Doctoral dissertation; 2015.
[31] Abuzaid W, Wu Y, Sidharth R, Brenne F, Alkan S, Vollmer M, et al. FeMnNiAl iron-based shape memory alloy: promises and challenges. Shape Memory and Superelasticity 2019;5(3):263–77. https://doi.org/10.1007/s40830-019-00230-9.
[32] Omori T, Iwaizako H, Kainuma R. Abnormal grain growth induced by cyclic heat treatment in Fe-Mn-Al-Ni superelastic alloy. Mater Des 2016;101:263–9. https://doi.org/10.1016/j.matdes.2016.04.011.
[33] Tseng LW, Ma J, Wang SJ, Karaman I, Chumlyakov YI. Effects of crystallographic orientation on the superelastic response of FeMnAlNi single crystals. Scripta Mater 2016;116:147–51. https://doi.org/10.1016/j.scriptamat.2016.01.032.
[34] Alaneme KK, Okotete EA. Reconciling viability and cost-effective shape memory alloy options – a review of copper and iron based shape memory metallic systems. Eng Sci Technol Int J 2016;19(3):1582–92. https://doi.org/10.1016/j.jestch.2016.05.010.
[35] La Roca P, Baruj A, Sade M. Shape-memory effect and pseudoelasticity in Fe–Mn-based alloys. Shap. Mem. Superelasticity 2017;3(1):37–48. https://doi.org/10.1007/s40830-016-0097-5.
[36] Hansen N. Hall–Petch relation and boundary strengthening. Scripta Mater 2004;51(8):801–6. https://doi.org/10.1016/j.scriptamat.2004.06.002.
[37] Liu H, Liu J, Michelic SK, Shen S, Su X, Wu B, et al. Characterization and analysis of non-metallic inclusions in low-carbon Fe-Mn-Si-Al TWIP steels. Steel Res Int 2016;87(12):1723–32. https://doi.org/10.1002/srin.201600131.
[38] Zhang L, Thomas BG. State of the art in the control of inclusions during steel ingot casting. Metall Mater Trans B 2006;37(5):733–61. https://doi.org/10.1007/s11663-006-0057-0.
[39] Ozcan H, Ma J, Wang SJ, Karaman I, Chumlyakov Y, Brown J, et al. Effects of cyclic heat treatment and aging on superelasticity in oligocrystalline Fe-Mn-Al-Ni shape

memory alloy wires. Scripta Mater 2017;134:66–70. https://doi.org/10.1016/j.scriptamat.2017.02.023.

[40] Vollmer M, Bauer A, Frenck J-M, Krooß P, Wetzel A, Middendorf B, et al. Novel prestressing applications in civil engineering structures enabled by Fe Mn Al Ni shape memory alloys. Eng Struct 2021;241(5972):112430. https://doi.org/10.1016/j.engstruct.2021.112430.

[41] Xia J, Omori T, Kainuma R. Abnormal grain growth in Fe–Mn–Al–Ni shape memory alloy with higher Al content. Scripta Mater 2020;187:355–9. https://doi.org/10.1016/j.scriptamat.2020.06.044.

[42] Omori T, Okano M, Kainuma R. Effect of grain size on superelasticity in Fe-Mn-Al-Ni shape memory alloy wire. Apl Mater 2013;1(3):32103. https://doi.org/10.1063/1.4820429.